Identification of Nonlinear Structural Elements by Force-State Mapping

Edward F. Crawley*
Massachusetts Institute of Technology, Cambridge, Massachusetts
and
Allan C. Aubert†
Cambridge Collaborative, Inc., Cambridge, Massachusetts

A major contributor to the passive damping and potentially nonlinear behavior of large space structures is the behavior of the joints. Proposed is an experimental technique called "force-state mapping" that will allow ground testing of these key structural elements. The technique includes the use of very accurate instrumentation to measure the force transmission properties of a structural element as a function of its mechanical state. When these data are presented in the form of a force-state map, the nonlinearities exhibit distinctively recognizable patterns. This presentation of the data allows the extraction of the describing parameters of the linear and nonlinear behavior and the energy dissipation characteristics of the joint. A series of tests were carried out on an idealized laboratory test article to demonstrate the technique. Strong structural nonlinearities, including a cubic hardening spring, friction, and impact phenomena, were introduced and measured. Parameters identified by the force-state mapping technique are compared with those made by traditional techniques and the errors involved in the measurement are estimated.

Introduction

MANY present and future orbital missions utilize structures or components that must be stored for launch, due to the limitations of the Shuttle payload bay. This requirement for storage implies that the subassemblies must be joined together, or deployed on orbit, to form the final assembled structure. The structural elements that perform this linking function—the joints—are seen to be a potential source of nonlinear behavior due to their discontinuous nature and complex load paths. These potential nonlinearities could impact the effectiveness of both systems identification and active control techniques. Further, they complicate the ground testing of space structures because of the inapplicability of the principle of linear superposition and they cloud the understanding of scaling laws for such structures.[1] Finally, the joints act as a primary location for passive energy dissipation, due to friction and impacting phenomena at the contact surfaces. A knowledge of the passive damping is especially important to the formulation of active control schemes.

A number of investigations into the effects of nonlinearities in structures have been performed. Several of these studies assess the applicability of testing methods based on assumptions of linear behavior to nonlinear systems.[2-6] The results show the possibility of detecting and quantifying certain selected weak nonlinearities in otherwise linear structures. Other testing techniques focus only on a particular type of nonlinearity, for instance, friction.[6-11] It is clear from these studies that no systematic testing technique yet exists that is capable of detecting and quantifying arbitrary nonlinear response in a structural element. Even the validity of 1*g* testing of space structures is in doubt, due to their expected nonlinear behavior.[12,13]

It is clear that the current state of technology is adequate in the area of the design and testing of structural elements, such as joints, with strong nonlinearities. It is the purpose of this study to investigate the applicability of a proposed technique called force-state mapping to the accurate measurement of linear and arbitrarily nonlinear properties in space truss joints. First, the motivation and theory of the force-state mapping method is explained and the expected results and benefits are presented. The experiment design with its idealizations and limitations will then be discussed. Finally, the results of a proof of concept experiment, as well as a discussion of their significance, will be presented.

Force-State Mapping Technique

The goal of this study is to develop an experimental technique that can identify and quantify the potentially nonlinear dynamic properties of space truss joints. As an example of the approach to be taken, the extensional dynamics of a simple boom-like space structure could be modeled by the lumped parameter system shown in Fig. 1. The spacecraft to the left is assumed to be a rigid body and the boom consists of joints and linear connecting elements that extend to the right. The joints are considered massless spring/dampers. These joints transmit force from one element to the next depending on their relative position and velocity, that is, depending on the mechanical state of the joint. The assumption that the joints are massless in comparison to the total mass of the structure is usually a good engineering approximation. The assumption that the force transmitted by the joint depends only on the state of the joint is rigorous, provided a sufficient number of states are included in the description of the joint. Particularly if memory effects are present in the dynamics of the joint, it may be necessary to include augmented states. However, no memory effects will be considered in the present discussion.

In order to determine the functional dependence of the transmitted force on its state, attention is focused on joint A in the structural model of Fig. 1. If, for simplicity, the spacecraft is assumed to be rigidly fixed and the boom con-

Presented as Paper 84-0992 at the AIAA/ASME/ASCE/AHS 25th Structures, Structural Dynamics and Materials Conference, Palm Springs, CA, May 14-16, 1984; received May 16, 1984; revision received May 16, 1985.

*Associate Professor of Aeronautics and Astronautics. Member AIAA.
†Scientist. Member AIAA.

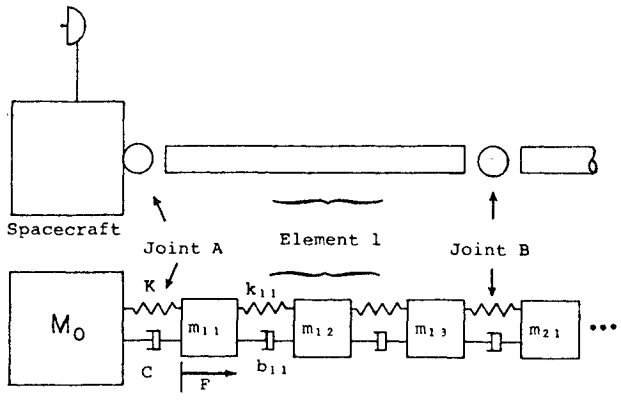

Fig. 1 Simplified model of jointed spacecraft boom.

sists only of lumped mass $m_{11}=M$, then the governing equation of motion is

$$M\ddot{x}=F-kx-C\dot{x} \tag{1}$$

where the terms on the right express the sum of the external and joint-dependent forces acting on the mass. In this form, the equation emphasizes the role of the joint as an element that applies a motion-dependent force to the remainder of the structure. If the characteristics of the joint are assumed to be arbitrarily nonlinear, then Eq. (1) can be rewritten as

$$M\ddot{x}=F-f(x,\dot{x}) \tag{2}$$

where f, the force produced by the joint, can be any function of displacement and velocity. This is the most general dynamic equation of motion for a single degree-of-freedom constant-mass system in the absence of memory effects. For emphasis, Eq. (2) can be rearranged as

$$f(x,\dot{x})=F-M\ddot{x}=F_{\text{NET}} \tag{3}$$

Therefore, the left-hand side of Eq. (3) represents a generalized displacement- and velocity-dependent net force emanating from the joint.

Equations such as Eq. (2) are normally solved in the direct sense, i.e., given initial conditions and a force time history, the time behavior of the states can be determined. However, the alternate form given in Eq. (3) can be used inversely. If the time history of the applied force and the acceleration are known, the force transmission characteristics of the joint can be determined as a function of its mechanical state. What is envisioned then is a three-dimensional plot of the net transmitted force ($F-M\ddot{x}$) vs displacement x and velocity $\dot{x}$. A plot of this type would be obtained by simultaneously measuring the force applied to the joint and its position, velocity, and acceleration. Each time the three position derivatives and the force are recorded, a point is produced in this three-dimensional space using Eq. (3). If the force transmitted is indeed only a function of the state, these individual measurements will form a repeatable surface. The nature and shape of the surface will be independent of the time history of the applied force. This surface of net transmitted force vs state is called a force-state map.

The useful feature of this data presentation format is that surface shapes resulting from most structural mechanisms are unique and recognizable. The ideal surface resulting from a linear spring is shown in Fig. 2. Note that the force is linear in x and that there is no variation in transmitted force with $\dot{x}$. Likewise, the force-state surface of a linear viscous damper would appear as a plane, with transmitted force varying linearly in $\dot{x}$ and with no variation of force in x. Thus, any combination of linear springs and dampers will yield a planar surface as its force-state map. As an example

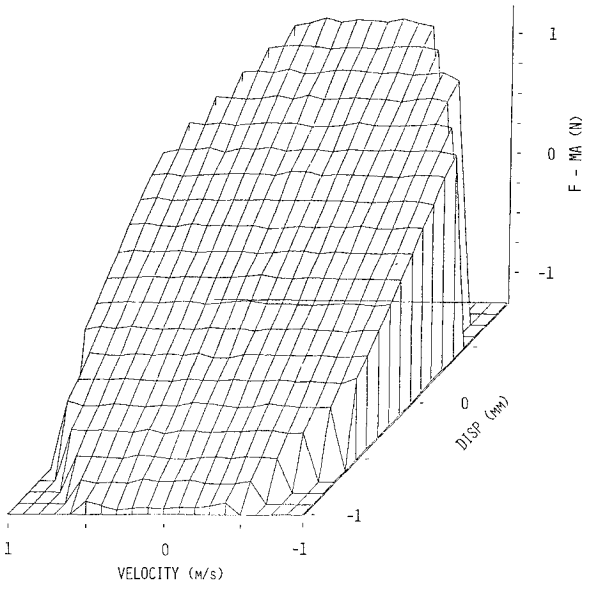

Fig. 2 Ideal linear spring force-state map.

of a nonlinear effect, a cubic hardening spring will produce response data such as is shown in Fig. 3. The cubic variation of force with x and an absence of variation with $\dot{x}$ are quite apparent. Finally, the surface shape resulting from classical friction is plotted in Fig. 4. In this model of simple Coulomb friction, the force has a fixed amplitude, which takes on the sign of the velocity.

The force transmission method is conceptually very simple in its assumptions and provides for a direct graphical presentation not provided by other methods. The next section will consider the practicality of the method as a testing technique and the factors involved with its implementation.

Experiment Design

In the previous section, it was indicated that four synchronized signals must be obtained for each degree of freedom: displacement, velocity, acceleration, and force. In principle, not all of the signals need to be measured directly since any of the time derivatives of position can be integrated or differentiated to yield the others. In practice, the need for accurate measurements, especially dictated by the requirement to differentiate force and acceleration to obtain net force and the difficulty of numerical differentiation, placed very stringent requirements on the accuracy and phase certainty of the experimental measurements. The practical implementation of a proof-of-concept experiment to demonstrate the force-state mapping technique is the subject of this section.

The force-state mapping technique was proposed to measure the structural characteristics in extension bending and shear of joints, such as the one shown in Fig. 5. However, such a joint would make for a difficult proof-of-concept experiment for several reasons. First, it would be difficult to modify in a controlled manner the nature and extent of the nonlinear behavior. Second, because of the unknown nature of the nonlinearity, it would be difficult to measure the joint response by conventional methods. This would make validation of the force-state technique impossible. Third, because of the highly complex behavior expected, such a test article may not meet the single-degree-of-freedom assumption present in the current formulation of the force-state technique.

As an alternative to using an actual joint as the proof-of-concept experiment, a reference test article was built that satisfies the single degree-of-freedom idealization and to which additional nonlinear elements can be successively added in a controlled manner. This consisted of a 2 kg test

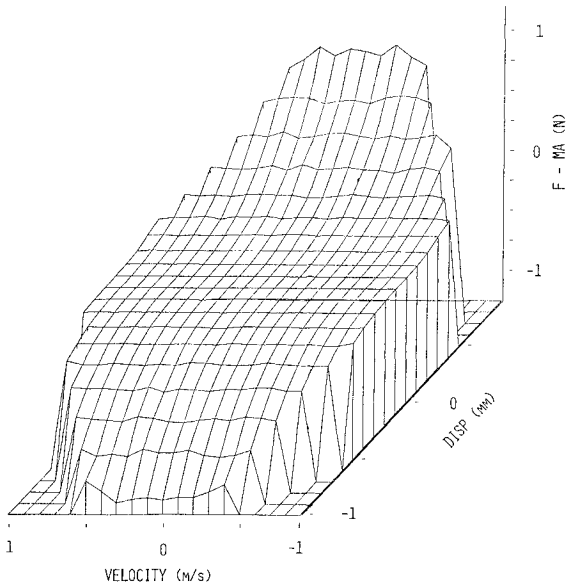

Fig. 3 Ideal cubic spring force-state map.

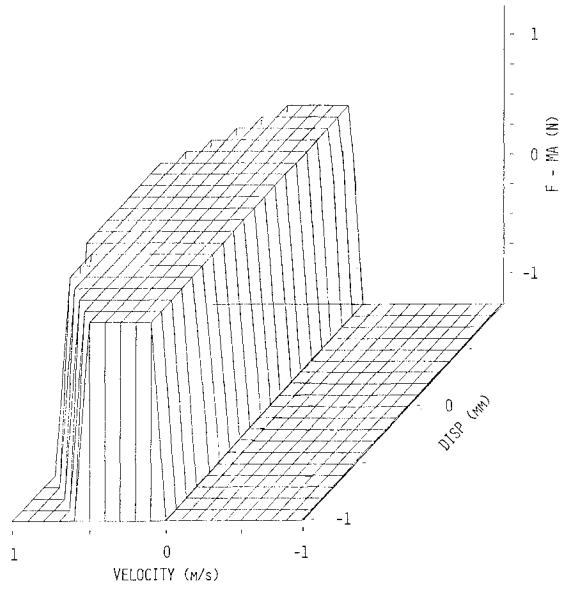

Fig. 4 Ideal Coulomb friction force-state map.

mass mounted on steel flexures and free to oscillate side to side in translation with a natural frequency of 11 Hz (Fig. 5b). Because of the orientation of the flexures, the mass had a preferred longitudinal axis of motion. With the resulting large modal separation in frequency, the reference test article behaved as a nearly perfect second-order undamped system. Various additional elements could be connected between the proof mass and adjacent rigid supports, which allowed nonlinear elements to be introduced into the dynamics of the system. These devices included "linear" air dampers, frictional surfaces, and impact bumpers. The details of these devices will be further discussed in the section on results. Figure 5b also illustrates the placement of the instruments and the forcing input, a 100 lb capacity Ling model 420 electromagnetic shaker.

In a very real way, the quality of the results from such an experiment can be only as good as the instruments and sensors used to measure the force input and response. Great pains were taken to select instrumentation and provide signal conditioning free of distortion and with high accuracy. Even

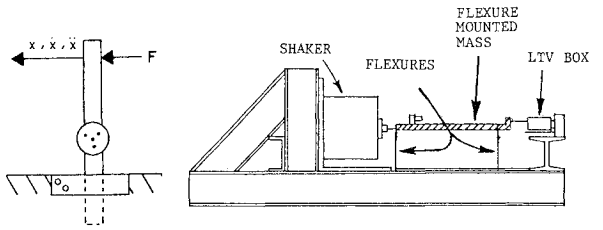

Fig. 5 Typical deployable locking hinge joint, and experimental setup showing shaker, reference test article, and transducer locations.

so, difficulties arose in calibrating the instruments and in controlling the signal noise content, especially in the measurement of net force. An error analysis showed that synchronization of different signals was also a critical factor.[14] These concerns and the selection of instrumentation to measure the displacement, velocity, acceleration, and force are discussed below.

Three types of displacement transducers were investigated: a linear variable differential transformer (LVDT), an inductive proximitor, and a variable capacitance transducer.[15] These devices were compared for their linearity, time or phase delay characteristics, and the stability of their zero reference. All three can be configured to provide acceptable linearity. The phase delay requirement was that there be a constant time delay, or linear phase delay, at any frequency. This would allow for eventual synchronization with the other signals. The proximitor time delay characteristics were unavailable and, for this reason, the device was rejected at that time. The capacitive device was more susceptible to noise and had a less stable zero reference than the LVDT. A repeatable zero displacement location is necessary in testing a nonlinear system in order to insure reproducibility in successive tests. Thus, the LVDT was chosen to measure displacement.

Only one applicable device was found that was appropriate for the velocity measurement. This device is called a linear velocity transducer (LVT). As its name implies, it provides a highly linear measurement of velocity from the voltage produced by mutual inductance. The device was simple and proved to have very good operating characteristics, accuracy, and drift characteristics. For these reasons, the LVT dynamic signal was used as the standard of comparison for all of the other instruments.

A wide range of laboratory accelerometers are available. For different types of accelerometers were considered: strain gage, piezoresistive, differential transformer, and piezoelectric. The strain gage and differential transformer devices did not meet the specified bandwidth requirements. The piezoelectric accelerometer is not well suited to low-frequency measurements and, in general, exhibited less linearity than the piezoresistive accelerometer, which was ultimately selected.

A low-sensitivity accelerometer was chosen, but it was susceptible to thermal drift. Consequently, great care was taken to observe the manufacturer's warmup recommendations. This drift would have rendered the device unacceptable if integration of the output had been required to yield velocity or displacement signals. However, the acceleration signal proved acceptable after postprocessing of the output removed any secular drift during the brief test time.

Piezoelectric strain gage force transducers were the options considered for the force measurement instrument. The strain gage device was rejected due to load range, bandwidth, and thermal sensitivity considerations. The piezoelectric device proved to have very good linearity and phase response and adequate low-frequency response.

An extensive error analysis was performed in order to predict the dominant system errors and noise sources. Error

bounds for the net force, as expressed by Eq. (3), were predicted for a linear undamped spring-mass system using the actual uncertainty errors measured for the instrument. The error bounds were calculated as a function of the ratio of driving frequency to the natural frequency of the system. Well below resonance, the error was dominated by that of the force transducer. At resonance, when the applied force is small, the error is roughly that of the accelerometer. However, above resonance, when the applied and inertial forces are similar in magnitude, the net force is the small difference between the two large numbers and the error grows large with respect to the signal. This indicates that the best signal-to-noise ratio is achieved at or below resonance. The trend of increasing noise level with increasing frequency above resonance will be evident in the results shown later in Figs. 7-9.

The error analysis indicated a need for highly synchronized measurements of the force, acceleration, and state in order that Eq. (3) be satisfied at any instant. Any instrument with frequency-dependent time delay (nonlinear phase shift) was excluded from consideration. An additional source of time delay, which can be frequency dependent, was the analog signal filtering. Four-pole Bessel filters, which have constant time delay characteristics, were employed. The requirement for synchronicity in the analog-to-digital conversion was satisfied by recording signals with a data logger capable of simultaneously sampling and holding up to 16 waveforms. The entire measurement system was carefully calibrated for synchronization by measuring the force, acceleration, velocity, and displacement of a 1 kg calibration proof mass. Each of the signals was compared to the others through a fourth-order Runge-Kutta integration to determine their relative time delay. Using these results, later test data were time shifted to correct for the instrument-related timing mismatches.

Initially each of the instruments was calibrated to an independent reference. However, during early runs, comparison of measurements showed calibration inconsistencies between the devices. It was decided to use the LVDT, calibrated by a micrometer, as the primary standard. The LVT was calibrated by comparison to the LVDT at low frequency and the accelerometer was calibrated by comparison with the LVT. The force calibration was then established by measuring the force and acceleration of the calibration proof mass. In this way, a consistent set of calibrations was obtained.

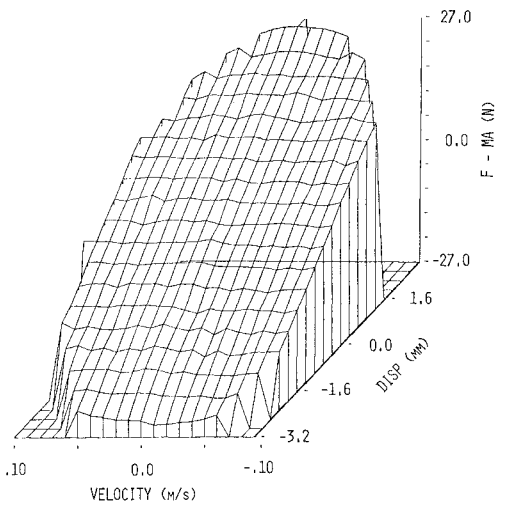

Fig. 6a Force-state map of reference spring mass test article driven at 5 Hz.

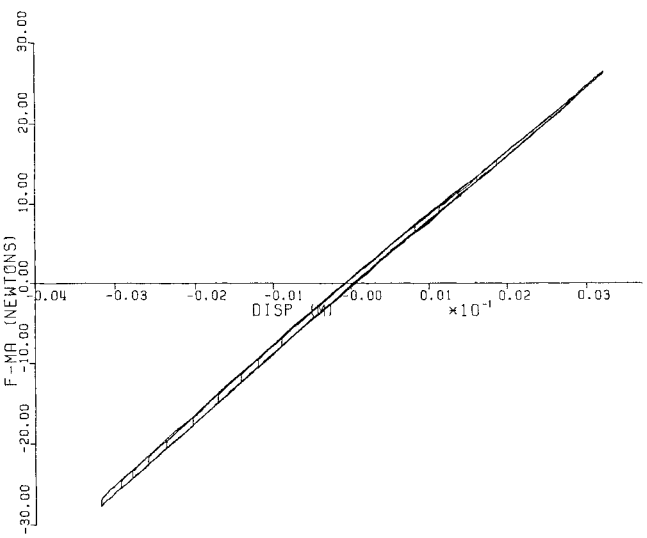

Fig. 6b Force vs displacement of the reference spring mass system driven at 5 Hz.

Experimental Results

Spring-Mass System

In order to verify its ability to identify linear and nonlinear structural characteristics, both individually and in combinations, the force-state mapping technique was applied to a series of structural systems built around the reference test article. The first tests were performed on the simple spring-mass reference test article with no additional elements added. The flexures that supported the mass provided a weak linear spring.

The three-dimensional force-state map for this spring-mass system is shown in Fig. 6a, in the same format as the idealized trends in Figs. 2-5. These data were obtained by digitally sampling the force and displacement derivatives, while driving the mass with with a ramped 5 Hz oscillatory input. This forcing input produced a spiraling contour in the force-state space. In such a sampling procedure, the values of the state $(x,\dot{x})$ at which data are sampled do not form a regular grid in displacement-velocity coordinates. The approach used in preparing figures such as Fig. 7a was to divide the peak to peak displacement and velocity ranges into 20 subranges, producing a 20×20 grid. All of the net force data taken within each of the 400 grid blocks were averaged and the values of the averages plotted. A more traditional presentation of the data is shown in Fig. 6b, which is equivalent to projecting the force-state surface on to the $\dot{x}=0$ plane. The small degree of hysteresis visible in Fig. 6b is due to friction in the LVT.

For purposes of comparison, two methods were used to make independent measurements of the spring stiffness. Both a static stiffness measurement and a free-vibration transient decay test were performed. The flexure stiffnesses and natural frequencies measured are shown in Table 1. They are compared with the value for the effective spring constant found by fitting a plane to the force-state map data using a least squares algorithm.[16] The force-state map result is within 4% of the other testing techniques and very close to their mean. The error analysis in Ref. 14 indicates that the upper bound on measurement error for this case is 2.76%. The agreement between the more reliable transient decay results and the force map result meets this expected accuracy, with only a 1.5% difference in the measured stiffnesses.

The three force maps presented in Figs. 6-8 show the effect on the signal-to-noise ratio of increasing the forcing frequency. All three show the same signal, the sloping characteristics of a linear spring. However, the apparent

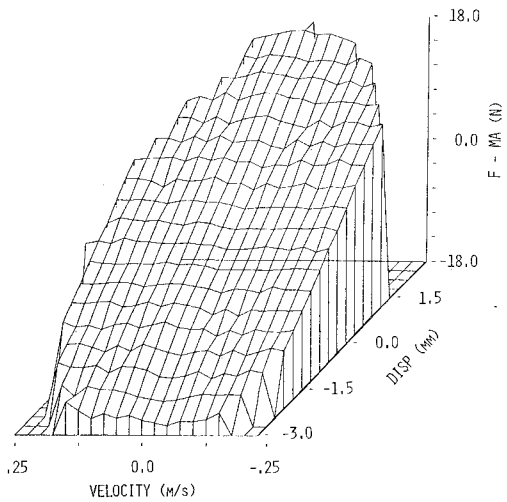

Fig. 7 Force-state map of the reference spring mass test article driven at 20 Hz.

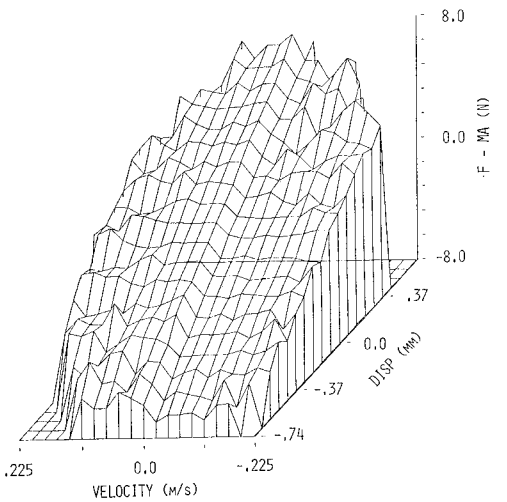

Fig. 8 Force-state map of the reference spring map test article driven at 50 Hz.

noise level increases with frequency, as was predicted by the error analysis. Since the tests are done at constant applied force rather than constant amplitude, the peak amplitude decreases with increasing frequency, further decreasing the signal-to-noise ratio. Since the higher-frequency plots are at lower signal level, smaller effects become more apparent. This is obvious in Fig. 8, where less than 1 N of friction force from the LVT can easily be identified as a clear step in the data in the vicinity of $\dot{x}=0$.

Viscous Damping

In an effort to introduce pure linear viscous damping, air dampers were next added to the basic spring-mass system. These devices have the classic piston and cylinder layout, which is so closely associated with "ideal" dampers, and use air as their working medium. There is an adjustable orifice through which the piston pumps air, creating the drag effect of the damper. For large orifice openings or low piston velocities, a linear viscous damper is closely simulated. Compressibility of the air becomes a significant factor for high piston velocities and/or small orifice openings.

The force-state characteristics of the air dashpot driven at 20 Hz are shown in Fig. 9, with a "light" damper setting. Note that, in addition to the expected linear dependence of force on velocity, two other trends are apparent: 1) there is a noticeable friction step at $\dot{x}=0$ and 2) there is a marked dependence of force on displacement, indicating that at 20 Hz and ± 2 mm amplitude the compressibility of the air is significant. Table 2 shows the results of a bench calibration of the damper, as well as results of fitting a plane to the force-state map derived at various frequencies. The damping values are seen to be in good agreement, the mean being almost exactly that given by the calibration. The increase in effective stiffness of the air dashpot with increasing frequency is also apparent.

Table 1 Flexure mounted mass properties

Technique	Flexure stiffness, N/m	Natural frequency, Hz
Static stiffness	7931	10.90
Free transient vibration test	8416	11.23
Force-state-map fit	8291	11.14

Table 2 Air damper response results, light damping

Technique	Damping, N·s/m	ω_0/Hz	Damper stiffness, N/m
Bench calibration	5.95	11.08	—
FMAP planar fit			
5 Hz	6.71	11.48	624
20 Hz	5.18	11.71	988
50 Hz	7.43	12.34	2032

Table 3 Coulomb friction results

Technique	Friction force, N
Calculated friction ($\mu=0.42$)	9.30
Transient decay (11 Hz)	3.96
FMAP planar fit	
5 Hz	7.02
20 Hz	5.05
50 Hz	4.62

Coulomb Friction

One of the suspected loss mechanisms in joints in space structures is Coulomb friction. To simulate this mechanism, an adjustable friction source was added to the spring-mass reference test article. The frictional contact surfaces were steel and the normal force was supplied by a spring with a set preload.

The force-state map is shown in Fig. 10 for the case of 20 Hz driving frequency. The linear effect of the flexure stiffness has been removed from this and subsequent plots. The force-state plot in Fig. 10 shows the step shape characteristic expected for Coulomb friction, in which the force is at a constant level with its sign determined by the velocity. A departure from the ideal Coulomb behaviour can be seen in the slight lag in the change of sign of the frictional force. Recall that a ramped decreasing oscillatory trajectory of x and $\dot{x}$ spirals in a clockwise direction in the three-dimensional view of Fig. 10. It can be seen that, as the trajectory on the high surface approaches the edge where the friction force changes sign, it crosses zero velocity and falls as it passes through two grid sectors until it reaches the lower surfaces. The magnitude of the force does not instantaneously change at zero velocity, but ramps to the new force value over the first 50 mm/s of velocity. This nonideal

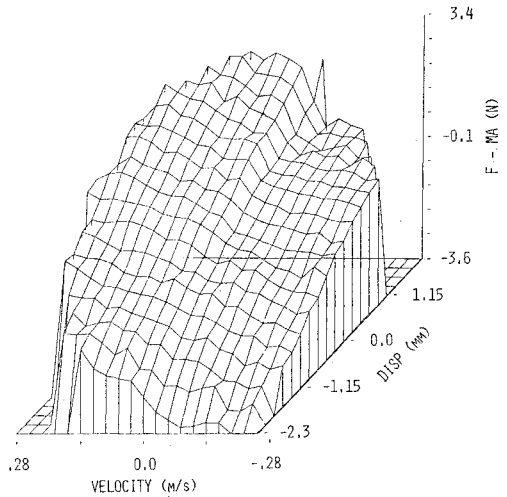

Fig. 9 Force-state map for an air dashpot damper driven at 20 Hz.

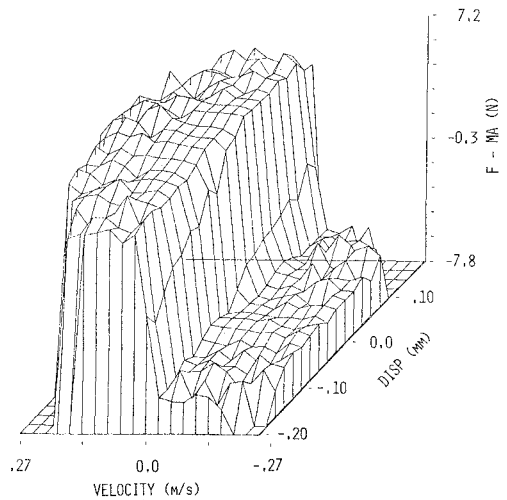

Fig. 10 Force-state map for friction dampers driven at 20 Hz.

behavior is probably due to the microslip and micromechanics of the friction surface. The trajectory continues around the lower surface, crosses zero velocity, and again rises through two grid sections to the upper level. This creates a discontinuity in the force at zero velocity/zero displacement, which is indicated in Fig. 11, but somewhat obscured by the data averaging used.

The ideal friction surface of Fig. 5 was fit by least squares to the surface of Fig. 10, resulting in the values of the friction listed in Table 3. There is a pronounced tendency for decreasing friction with increasing forcing frequency. For comparative purposes, the frictional force was estimated, based on a handbook friction coefficient of $\mu = 0.42$ and a normal spring preload of 22 N, and was back calculated from a transient decay measurement. Comparison of the results shows moderate agreement; however, the difficulty of making any accurate measurement of siding friction cannot be underestimated.

Cubic Spring

It is suspected that joints which are part of deployment mechanisms will have deadbands, one manifestation of which will be a nonlinear stiffness. In order to introduce a strong but continuous nonlinear stiffness, a cubic spring was added to the reference test article. The spring was a simple piece of steel wire whose axis of preload was normal to the axis of the single degree of motion of the reference test article.

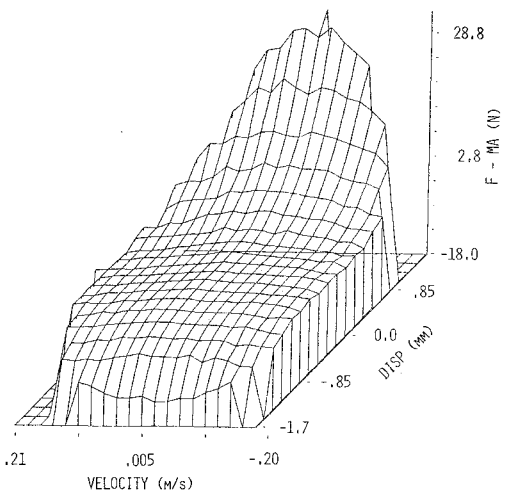

Fig. 11 Force-state map for a cubic spring driven at 20 Hz.

Figure 11 shows the force-state map of the system driven at 20 Hz. Again, the results have the linear influence of the spring flexures removed. A hardening region is evident for both positive and negative deflections, with little variation of force with velocity. A cubic stiffness value was obtained by fitting a cubic surface in the data of Fig. 11. The resulting stiffness of 45×10^8 N/m^3 was not in good agreement with the theoretical value, probably due to an initial lack of tension in the wire.

Impact Phenomena

Impact phenomena are another by-product of deadbands occurring in joints. To simulate the impact occurring as a deadband closes, a set of "bumpers" was added to the reference test article. The aluminum bumpers were covered with a ¼ in. thick rubber sheet to create a "soft" impact. To most closely simulate the conditions expected in a real joint, the Coulomb friction device was also included in this test. A second objective of this test was, therefore, to determine how these two nonlinearities, friction plus impacting, superimpose and how easily their individual contribution can be detected.

The results of this configuration, when driven at 20 Hz, are shown on the force-state map in Fig. 12a and projected onto the $\dot{x} = 0$ plane in Fig. 12b. As expected, there is a region on either side of zero displacement with no change in force and then a sharp stiffening onset as the deadband closes and the bumper makes contact. The energy dissipation associated with the impact is clearly seen as the area within the loop at the limits of displacement in Fig. 12b. The presence of the friction is evident by the fact that the negative velocity trajectory is at a lower steady force level than the positive velocity trajectory.

The same observations can be made by examining the force-state map in Fig. 12a. It can be seen that, in the regions of bumper contact, the slopes of the constant velocity lines show a sharp slope of force proportional to the displacement. This is the stiffness component of the bumpers. Also, the constant-displacement lines show a slope of force with velocity, especially in the region where the velocity has changed to the opposite sign of the displacement. The small but noticeable step in force at zero velocity is due to the friction. Thus, in force-state space, the superposition of these two nonlinear effects is seen to take place in an understandable manner, allowing ready identification of the system characteristics.

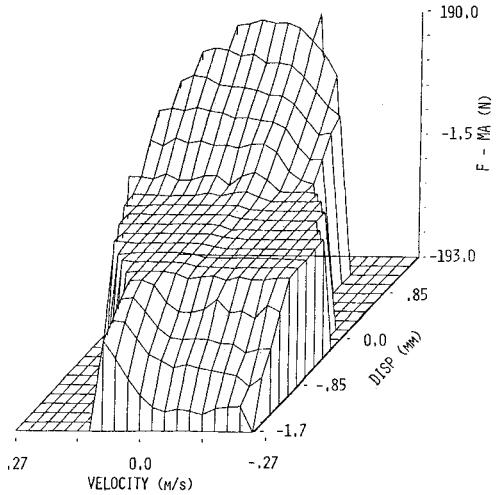

Fig. 12a Force-state map for friction plus impact bumpers driven at 20 Hz.

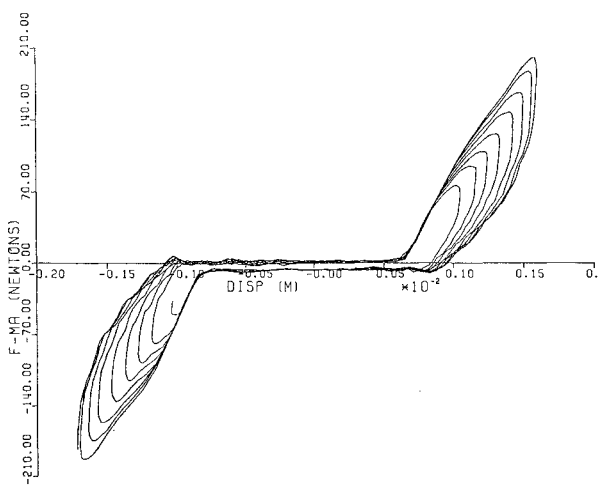

Fig. 12b Force vs displacement for friction plus impact bumpers driven at 20 Hz.

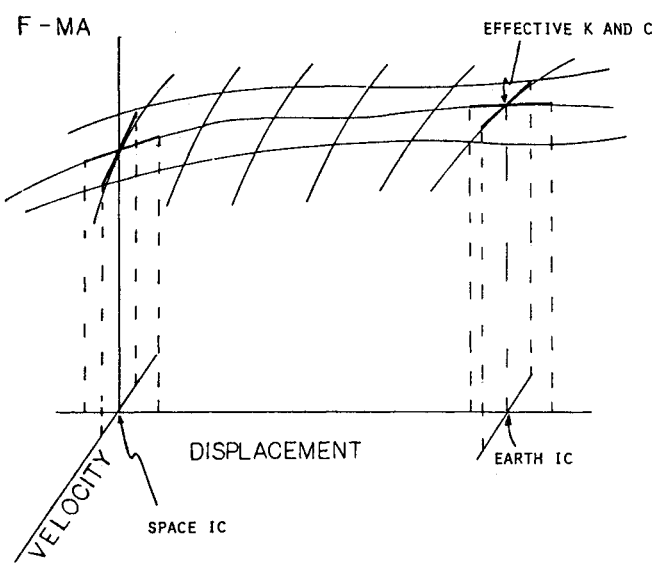

Fig. 13 Use of the force-state map to determine the effective stiffness and damping in a jointed structure as would be measured on Earth and in space.

Conclusions and Discussion

A technique has been developed in rudimentary form and demonstrated on a simple test article for the direct identification of nonlinearities in structural components such as joints. The advantages of the force-state mapping technique are its ability to handle arbitrarily strong nonlinearities and the direct graphical form of the data presentation. By either fitting a known surface to the data or storing the data in a lookup table, the force transmission characteristics of the joint are available for use in time-marching calculations of the response of structures in which the joint was included.

As an alternative to the direct use of the force-state data, equivalent or effective stiffness and damping parameters can be extracted for small-amplitude vibration. As an example, the left side of Eq. (3) can be expanded into a Taylor series about an arbitrary reference state, $x_0, \dot{x}_0$ as

$$f(x,\dot{x}) = f(x_0,\dot{x}_0) + (x-x_0)\frac{\partial f}{\partial x}\bigg|_{x_0,\dot{x}_0} + (\dot{x}-\dot{x}_0)\frac{\partial f}{\partial \dot{x}}\bigg|_{x_0,\dot{x}_0} + \ldots \tag{4}$$

where the derivatives are just the local slopes of the surface (Fig. 13). For a small region around the $x_0, \dot{x}_0$ location, the slopes represent the coefficients of the complex tangent modulus or the "local" damping and stiffness. Alternatively, a local complex secant modulus could be defined to express the correct average stiffness and energy dissipation over a given amplitude of vibration about a reference state.

Figure 13 shows an interesting application of the force-state map to Earth testing of space structures. Suppose a structure was suspended in 1 g in such a way that the gravity load caused a steady deflection. The small displacement vibration would then take place about this "Earth IC" (Fig. 13) and would have the effective stiffness and damping shown. In space, in the absence of gravity loads, there would be no steady deflection and the effective K and C would be about a "Space IC," as shown. For a generally nonlinear joint, these properties could be completely different from those of the Earth test, leading to differences in dynamic behavior on orbit when compared to those measured on Earth.

Acknowledgments

The authors wish to acknowledge the support of NASA under Grant NAGW-21, with Mr. Samuel Venneri of NASA Headquarters serving as Technical Monitor. They also wish to acknowledge the assistance of Mr. Kevin J. O'Donnell in the completion of the experimental effort.

References

[1]Hertz, T. J. and Crawley, E. F., "Damping in Space Structure Joints," AIAA Paper 84-1039, May 1984.

[2]Tomlinson, G. R., "An Analysis of the Distortion Effects of Coulomb Damping on the Vector Plots of Lightly Damped Systems," *Journal of Sound and Vibration,* Vol. 71, Aug. 1980, pp. 443-451.

[3]Ibrahim, S. R., "Time-Domain Quasi-Linear Identification of Nonlinear Dynamic Systems," AIAA Paper 83-0811, May 1983.

[4]Horta, L. G. and Hanks, B. R., "A Study of the Effects of a Cubic Nonlinearity on a Modern Modal Identification Technique," AIAA Paper 83-0810, May 1983.

[5]Ewins, D.J. and Sidhu, J., "Modal Testing and the Linearity of Structure," *Mecanique Materiaux Electricite,* Nos. 389-390-391, May-June-July 1982, pp. 297-302.

[6]Tomlinson, G. R. and Hibbert, J. H., "Identification of the Dynamic Characteristics of a Structure with Coulomb Friction," *Journal of Sound and Vibration,* Vol. 64, May 1979, pp. 233-242.

[7]Villaggio, P., "An Elastic Theory of Coulomb Friction," *Archive for Rational Mechanics and Analysis,* Vol. 70, No. 2, 1979, pp. 135-143.

[8]Bielawa, R. L., "An Analytic Study of the Energy Dissipation of Turbomachines Bladed-Disk Assemblies Due to Inter-shroud Segment Rubbing,' *Journal of Mechanical Design, Transactions of ASME,* Vol. 100, April 1978, pp. 222-228.

[9]Alspaugh, D. W., "Analysis of Coulomb Friction Vibration Dampers," *Journal of Sound and Vibration,* Vol. 57, March 1978, pp. 65-78.

[10]Crawley, E. F., Sarver, G. L., and Mohr, D. G., "Experimental Measurements of Passive Materials and Structural Damping for Flexible Space Structures," *Acta Astronautica,* Vol. 10, No. 5-6, May-June 1983, pp. 381-393.

[11]Sinha, A. and Griffin, J. H., "Effects of Friction Dampers on Aerodynamically Unstable Rotor Stages," AIAA Paper 83-0848, May 1983.

[12]Crawley, E. F. and Mohr, D. G., "Experimental Measurement of Material Damping in Free Fall with Tuneable Excitation," *AIAA Journal,* Vol. 23, Jan. 1985, pp. 125-131.

[13]Hanks, B. R. and Pinson, L. D., "Large Space Structures Raise Testing Challenges," *Astronautics and Aeronautics,* Vol. 21, Oct. 1983, pp. 34-40.

[14]Aubert, A. C., Crawley, E. F., and O'Donnell, K. J., "Measurement of the Dynamic Properties of Joints in Flexible Space Structures," Space Systems Laboratory, Massachusetts Institute of Technology, Cambridge, Rept. 35-83, Sept. 1983.

[15]Doebelin, E. O., *Measurement Systems, Application and Design,* McGraw-Hill Book Co., New York, 1975.

[16]Marquardt, D. W., "An Algorithm for Least-Squares Estimation of Nonlinear Parameters," *Journal of the Society for Industrial and Applied Mathematics,* Vol. 11, No. 2, 1963, pp. 431-441.